

6 The performance of nitrate-reducing Fe(II) oxidation processes 7 under variable initial Fe/N ratios: The fate of nitrogen and iron 8 species

9 Boyi Cheng¹, Yi Wang¹, Yumei Hua (✉)¹, Kate V. Heal²

10 ¹ College of Resources and Environment, Huazhong Agricultural University, Wuhan 430070, China

11 ² School of GeoSciences, University of Edinburgh, Edinburgh EH9 3FF, UK

12

13 © Higher Education Press 2020

14

15

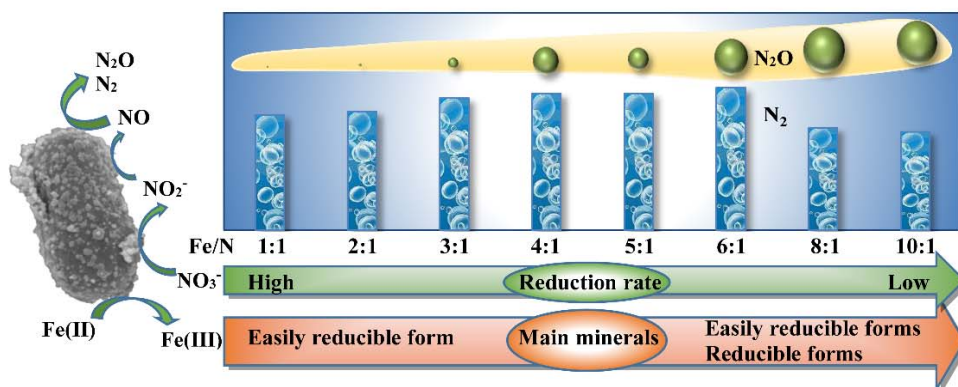
16 HIGHLIGHTS

17

- 18 • Bacterially-mediated coupled N and Fe processes examined in incubation experiments.
- 19 • NO_3^- reduction was considerably inhibited as initial Fe/N ratio increased.
- 20 • The maximum production of N_2 occurred at an initial Fe/N molar ratio of 6.
- 21 • Fe minerals produced at Fe/N ratios of 1–2 were mainly easily reducible oxides.

22

23 GRAPHIC ABSTRACT



24

25

26

27 ABSTRACT

28 The Fe/N ratio is an important control on nitrate-reducing Fe(II) oxidation processes that occur both in the aquatic
29 environment and in wastewater treatment systems. The response of nitrate reduction, Fe oxidation, and mineral
30 production to different initial Fe/N molar ratios in the presence of *Paracoccus denitrificans* was investigated in
31 132 h incubation experiments. A decrease in the nitrate reduction rate at 12 h occurred as the Fe/N ratio increased.
32 Accumulated nitrite concentration at Fe/N ratios of 2–10 peaked at 12–84 h, and then decreased continuously to
33 less than 0.1 mmol/L at the end of incubation. N₂O emission was promoted by high Fe/N ratios. Maximum
34 production of N₂ occurred at a Fe/N ratio of 6, in parallel with the highest mole proportion of N₂ resulting from
35 the reduction of nitrate (81.2%). XRD analysis and sequential extraction demonstrated that the main Fe minerals
36 obtained from Fe(II) oxidation were easily reducible oxides such as ferrihydrite (at Fe/N ratios of 1–2), and easily
37 reducible oxides and reducible oxides (at Fe/N ratios of 3–10). The results suggest that Fe/N ratio potentially
38 plays a critical role in regulating N₂, N₂O emissions and Fe mineral formation in nitrate-reducing Fe(II) oxidation
39 processes.

40

41 ARTICLE INFO

42 *Article history:*

43 Received April 9, 2020, Revised September 29, 2020, Accepted September 30, 2020, Available online November
44 14, 2020

45 **Keywords:**

46 Denitrification, N₂O emission, Fe(II) oxidation, Fe/N ratio, Fe minerals

47

48

49 1 Introduction

50

51 An excess presence of NO₃⁻ is harmful for aquatic ecosystems and human health, and hence NO₃⁻ removal has
52 been the focus of many research efforts in natural aquatic environments and wastewater treatment (Zorgani et al.,
53 2016; Han et al., 2019; Zhang et al., 2019). Biological denitrification is the main process of NO₃⁻ removal, for
54 which the traditional electron donor is organic carbon. Inorganic substrates such as sulfur and Fe compounds can
55 also act as electron donors for NO₃⁻ reduction (Melton et al., 2014). Fe is an abundant element in the environment,
56 and plays an important role in both Fe and N cycles through nitrate-reducing Fe(II) oxidation (NRFO) bacteria
57 (Straub et al., 1996; Weber et al., 2006; Melton et al., 2014). The contribution of NRFO to anoxic Fe(II) oxidation
58 and the subsequent behavior is of great importance as NRFO bacteria have been discovered in a variety of habitats
59 globally (Weber et al., 2006; Zhang et al., 2015).

60 Autotrophic N removal technologies mediated by NRFO bacteria have the advantage of minimising secondary
61 pollution risk and have shown promise, especially for wastewater with a low C/N ratio (Zhang et al., 2014).

62 However, autotrophic cultures based only on NO_3^- and Fe(II) generally result in slow growth of NRFO bacteria,
63 while mixotrophic cultures based on NO_3^- , Fe(II) and organic cosubstrate (e.g., acetate) result in fast growth
64 (Chakraborty et al., 2011; Jamieson et al., 2018). Moreover, most NRFO bacteria are described as mixotrophic
65 (Klueglein and Kappler, 2013), such as *Paracoccus denitrificans* which was demonstrated to oxidize 84% of
66 Fe(II) with an initial concentration of 4.5 mmol/L and reduce 0.7 mmol/L nitrate simultaneously in a pure culture
67 (Muehe et al., 2009). As sediment in freshwater ecosystems contains accumulated organic carbon, mixotrophic
68 NRFO bacteria may be predominant and play a significant role in the microbially mediated transformation of
69 Fe(II) to Fe(III) in aquatic anoxic environments. Here, NO_3^- acts as the preferred electron acceptor based on
70 energy considerations, and reactions between Fe and N may predominate (Melton et al., 2014; Liu et al., 2019).

71 Denitrification is a four-step reductive process through which NO_3^- is sequentially transformed into NO_2^- , NO,
72 N_2O , and finally N_2 (Sparacino-Watkins et al., 2014), with the different products posing different impacts on
73 human health and the environment. NO_2^- can cause methemoglobinemia and respiratory infections in humans
74 (Watsuntorn et al., 2019). N_2O has a long atmospheric residence time of 114 years, behaves as a potent
75 “greenhouse” gas and is the most significant contributor to stratospheric ozone depletion, negatively affecting
76 human health, sensitive aquatic organisms and ecosystems (Zhu-Barker et al., 2015; Vasilaki et al., 2018). In
77 contrast, N_2 does not have significant negative impacts and is the most desirable product of NO_3^- reduction.
78 Hence, more detailed knowledge of the processes involved in N transformation could help to improve
79 understanding of the NRFO process and inform management of denitrification to minimise its negative by-
80 products.

81 The reduction of NO_3^- by mixotrophic NRFO bacteria is coupled with the oxidation of Fe(II), resulting in the
82 formation of various Fe (hydr)oxide minerals (Miot et al., 2015; Jamieson et al., 2018). The Fe minerals formed
83 include ferrihydrite, green rust, goethite, lepidocrocite and magnetite, depending on various growth conditions
84 (Posth et al., 2014). For example, *Acidovorax* sp. Strain BoFeN1, a strain of NRFO bacteria, is able to form
85 different types of Fe minerals (Miot et al., 2009b), e.g., green rust (Klueglein and Kappler, 2013), goethite
86 (Larese-Casanova et al., 2010) and lepidocrocite (Liu et al., 2019), under different conditions. Fe minerals can
87 precipitate on the surface of bacteria and decrease the metabolic efficiency of NO_3^- reduction (Miot et al., 2015;
88 Chen et al., 2018). However, Fe minerals also provide a positive control on the cycling of contaminants such as
89 phosphorus and metal/metalloids, through their adsorption on Fe minerals with a high specific surface area
90 (Pownceby et al., 2019), thus influencing the transport and fate of these species in natural environments and
91 wastewater treatment systems. Since the adsorption capacity of Fe minerals together with their environmental
92 behavior are related to their mineralogy, it is important to identify the Fe minerals produced in the NRFO process.

93 According to theoretical equations, Fe/N molar ratios may affect the products of NO_3^- reduction during the
94 NRFO process through the catalysis of some chemicals including Fe(III) (hydr)oxide minerals, green rust, pyrite,
95 and Cu^{2+} (Straub et al., 1996; Ottley et al., 1997; Picardal, 2012), and subsequently the environmental impact of
96 different denitrification products. Conversely, Fe minerals with different effective behaviors for removing toxic
97 metals (e.g., As and Cr) and phosphorus during Fe(II) oxidation may also be produced at different Fe/N ratios.
98 The effect of Fe/N molar ratios (1–6) on NO_3^- removal efficiency has been reported (Zhang et al., 2014), but the
99 denitrification products (i.e., NO_2^- , N_2O and N_2) and Fe minerals mediated by Fe/N molar ratio have not been
100 clarified yet. Hence, using *Paracoccus denitrificans* the current research aims to investigate the performance of
101 NRFO at different initial Fe/N molar ratios, during which the products in the headspace gas, aqueous phase and
102 precipitates were investigated to explore the fate of N and Fe.

103

104

105 2 Materials and methods

106

107 2.1 Bacterial strain and medium

108

109 *Paracoccus denitrificans* (CCTCC AB2013117) was purchased from China Center for Type Culture Collection
110 and first activated in a beef extract-peptone medium at 30°C. The bacteria were cultured to the exponential phase
111 using the spread plate method, reaching a concentration of 1.5×10^8 cell/mL. The cells were harvested by
112 centrifugation (5000 r/min, 30 min, 30°C), washed twice with a PIPES buffer (10 mmol/L, pH 7.0), and then
113 resuspended as an inoculum for the different experimental treatments.

114 The experimental medium solution, containing 0.3 g/L NH_4Cl , 0.5 g/L KH_2PO_4 , 0.1 g/L $\text{CaCl}_2 \cdot 2\text{H}_2\text{O}$, and 0.5
115 g/L $\text{MgSO}_4 \cdot 7\text{H}_2\text{O}$, was autoclaved and cooled. Then NaHCO_3 solution, trace element mixture SL8, vitamins, and
116 sodium acetate solution were filter-sterilized (0.22 μm), placed in a UV sterilization station (SW-CJ-2FD, China)
117 and added (Ehrenreich and Widdel, 1994; Muehe et al., 2009), so that the initial sodium acetate concentration in
118 the medium was 1 mmol/L. The medium pH was adjusted to 7.0 with NaOH solution (~ 0.1 mol/L) in a UV
119 sterilization station (SW-CJ-2FD, China).

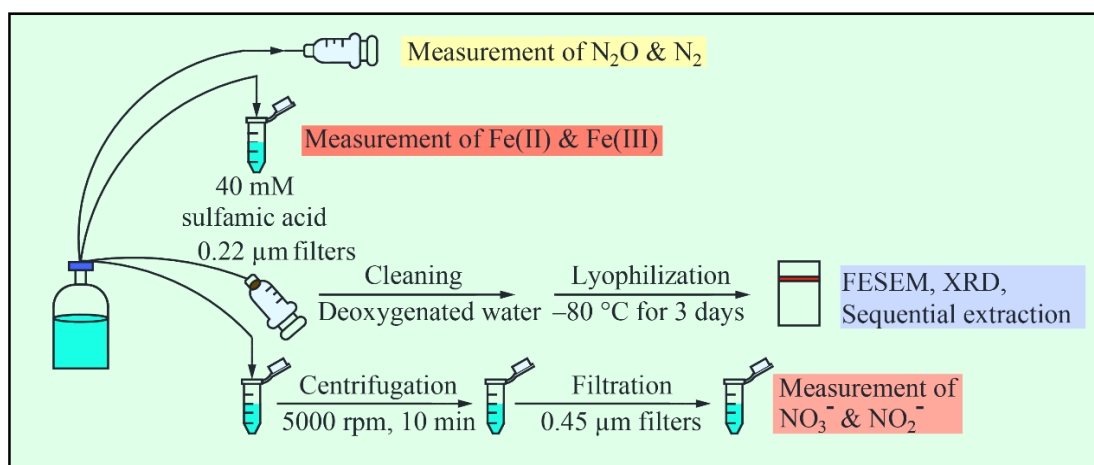
120

121 2.2 Experimental procedure

122

123 Five mL of cell suspension were added to 118-mL serum bottles containing 93 mL of medium deoxygenated by
124 O_2 -free ultrapure Ar gas. Eight treatments were set up as follows. The parallel serum bottles were purged with O_2 -
125 free ultrapure Ar gas for at least 2 min (0.6 L/min flux) to replace the headspace air. The NO_3^- concentration in all
126 bottles was 1 mmol/L from the addition of 1 mL NaNO_3 solution. One mL $\text{FeSO}_4 \cdot 7\text{H}_2\text{O}$ solution was added at
127 concentrations of 100, 200, 300, 400, 500, 600, 800, and 1000 mmol/L in each bottle separately before the end of
128 the Ar gas purging, resulting in initial Fe/N molar ratios of 1, 2, 3, 4, 5, 6, 8, and 10. The Fe(II) stock solutions
129 were prepared by adding $\text{FeSO}_4 \cdot 7\text{H}_2\text{O}$ to anoxic (100% Ar headspace) deoxygenated water and then sealing the
130 bottle with a butyl stopper under an anoxic atmosphere (100% Ar headspace). The time at which the incubation
131 bottles were quickly sealed with butyl rubber septa and an aluminum crimp was recorded as 0 h. Two needles
132 fitted with a three-way valve were inserted into each butyl rubber septa for gas and solution sampling,
133 respectively. At 0, 12, 36, 60, 84, 108, and 132 h, serum bottles for each set of treatments were removed for
134 destructive sampling to determine the pH, as well as the NO_3^- , NO_2^- , Fe(II), Fe(III), and dissolved organic carbon
135 (DOC) contents (Fig. 1). Precipitate samples were collected at the end of the experiment at 132 h via a filter
136 syringe (0.22 μm). Then, the precipitates collected on 0.22 μm filter were washed twice with deoxygenated water
137 and freeze-dried (-80°C) (SCIENTZ-18N, China) before determination of different Fe fractions. All experiments
138 were performed in triplicate and cultivated at 30°C.

139



140

141 **Fig. 1** Schematic representation of the sampling and pretreatment processes for gas, liquids, and precipitates from the experimental
 142 bottles.

143

144 2.3 Sample analysis and calculations

145

146 The ferrozine assay was used to determine the concentration of Fe(II) in the dissolved phase, after mixing sampled
 147 culture suspensions with 40 mmol/L sulfamic acid (pH~1.8) (Klueglein and Kappler, 2013). Total Fe content was
 148 determined by reducing an aliquot of the sample with hydroxylamine hydrochloride before addition of the
 149 ferrozine reagent (Stookey, 1970). Fe(III) content was calculated by subtracting the Fe(II) content from the total
 150 Fe content. A pH meter (Mettler Toledo, Switzerland) was used to determine the pH value. Other suspension
 151 samples were placed in an UV sterilization station to kill all cells (SW-CJ-2FD, China) and then fully exposed to
 152 O₂, to induce oxidation of Fe(II) (Chen et al., 2018). Subsequently, they were centrifuged (5000 r/min, 10 min)
 153 to remove both the cells and the Fe oxides and then filtered through a 0.45 μm membrane before determination of
 154 NO₃⁻-N, NO₂⁻-N (APHA, 2012) and DOC concentrations using a total organic carbon analyzer (Vario TOC cube,
 155 Elementar, Germany).

156 Contents of N₂O and N₂ in headspace samples were determined by gas chromatography using an Agilent
 157 7890A (USA) equipped with an electron capture detector and an Agilent 7890B (USA), respectively.

158 The morphology of the precipitates was investigated using a field emission scanning electron microscope
 159 (FESEM, GeminiSEM 300, Germany) at 5 kV. The type of Fe minerals in the precipitates was identified with an
 160 X-ray diffractometer (Bruker, Germany) using Cu Kα filtered radiation. The precipitate samples were scanned
 161 between 5 and 80° 2θ using a step size of 0.02° and a scan speed of 1.0° 2θ/min. MDI Jade 6.5 was used to
 162 identify the mineral phases. A sequential extraction procedure (Fig. A1; Ma et al., 2019) was applied to the
 163 precipitates to fractionate Fe into the following forms: carbonate associated (Fe_{carb}), easily reducible oxides
 164 (Fe_{ox1}), reducible oxides (Fe_{ox2}), magnetite (Fe_{mag}), poorly reactive sheet silicate (Fe_{prs}), and unreactive silicate
 165 (Fe_U) (Poulton and Canfield, 2005; Ma et al., 2019). Fe concentration was determined using ferrozine method
 166 (Stookey, 1970) in aliquots of the solution resulting from each extraction step. Additionally, total Fe was extracted
 167 from the precipitate using 0.5 mol/L HCl (Wang et al., 2016) and measured with the ferrozine method (Stookey,
 168 1970).

169

170 2.4 Statistical analysis

171

172 Duncan's multiple range tests were performed using SPSS 20.0 software (USA) to identify any significant
173 differences between samples. Correlative analyses were performed using Pearson's correlation.

174

175

176 3 Results

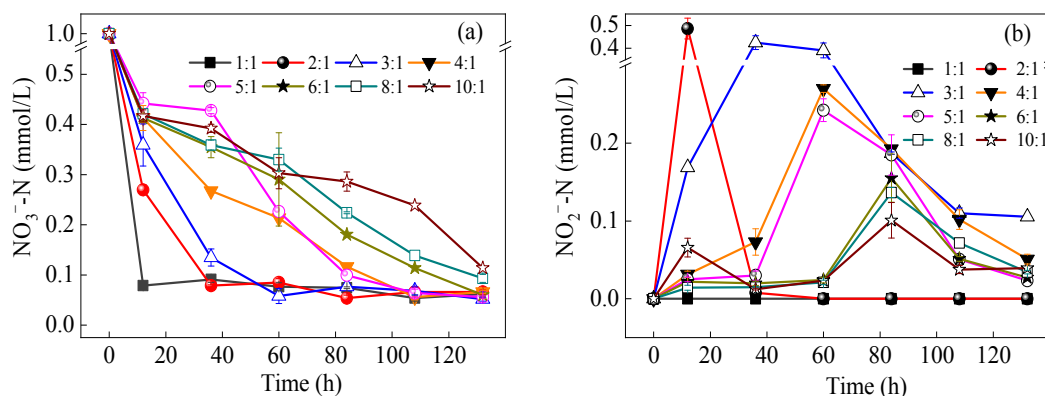
177

178 3.1 Variation in NO_3^- and NO_2^- concentrations

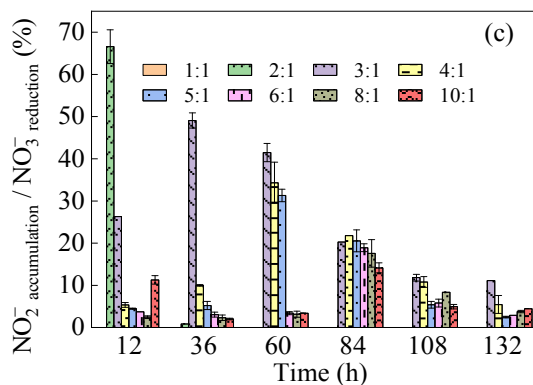
179

180 Generally, the NO_3^- concentration in all treatments decreased with time (Fig. 2(a)). At 12 h, the NO_3^-
181 concentration was very similar (0.41–0.44 mmol/L) for treatments with Fe/N ratios of 4–10, but was only 0.08
182 mmol/L at Fe/N ratio of 1. NO_3^- reduction rates at 12 h in treatments with Fe/N ratio of 1 and 2 (76.8 and 60.9
183 $\mu\text{mol/L/h}$ respectively) were higher than in treatments with Fe/N ratios of 4–10 (46.5–53.4 $\mu\text{mol/L/h}$). At the end
184 of the incubation, the reduction in the initial NO_3^- concentration was ~95%, except for in the treatments with Fe/N
185 ratios of 8 and 10, which had significantly lower NO_3^- consumption than other treatments (Table A1).

186



187

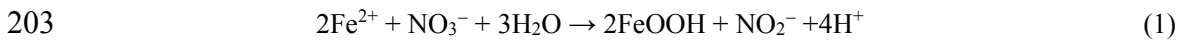


188

189 **Fig. 2** NO₃⁻ concentration (a), NO₂⁻ concentration (b), and NO₂⁻ accumulation expressed as a % of NO₃⁻ reduction (c) during the
190 incubation. The NO₂⁻ concentration at a Fe/N ratio of 1 was zero throughout the incubation, and that at a Fe/N ratio of 2 fell to zero
191 after 36 h. Values are means (*n* = 3) and error bars in (a) and (b) represent the standard deviation.

192

193 The timing and magnitude of peak NO₂⁻ concentration, a common intermediate of denitrification, varied
194 between treatments with different Fe/N ratios (Fig. 2(b)). The detection of no NO₂⁻ in the Fe/N ratio 1 treatment
195 was probably attributed to the fast reduction with a suitable pH of this treatment (Fig. A2) (Buchwald et al., 2016)
196 and the lower inhibiting effect on cell growth by Fe mineral encrustation. NO₂⁻ accumulation was detected at
197 Fe/N ratios of 2–10, first increasing and then decreasing, with peak magnitude decreasing and peak timing
198 increasing as Fe/N ratio increased from 2 to 10. A similar pattern was evident in NO₂⁻ accumulation expressed as
199 a % of NO₃⁻ reduction during the incubation (Fig. 2(c)). The peak percentage of NO₂⁻ to NO₃⁻ reduction was
200 66.6% for the Fe/N ratio 2 treatment at 12 h, much higher than that for other treatments, while the peak percentage
201 for Fe/N ratios of 3–5 occurred during 12–60 h. The initial Fe/N ratio of 2 would favor NO₂⁻ production from a
202 stoichiometric point of view (Ottley et al., 1997) as illustrated in Eq. (1):



204 A large NO₂⁻ accumulation (equivalent to > 30% of the reduced NO₃⁻) was observed at Fe/N ratios of 2–5
205 within 60 h, but at 132 h NO₂⁻ concentrations in all Fe/N ratio treatments were below 0.11 mmol/L.

206

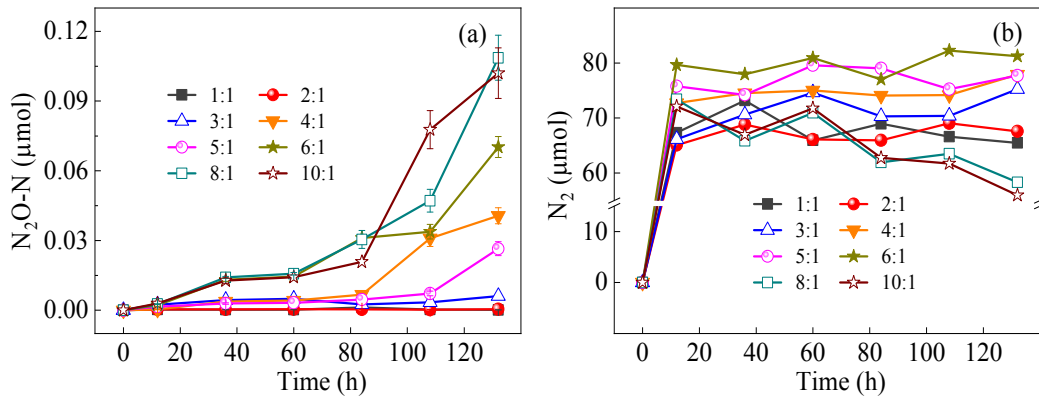
207 3.2 N₂O and N₂ emissions

208

209 The N₂O production in the headspace was below 0.006 μmol at Fe/N ratios of 1–3 throughout the incubation,
210 while it generally showed an increasing tendency at Fe/N ratios of 4–10 (Fig. 3(a)). By comparison, the N₂O
211 production at the Fe/N ratio of 10 at 12 h was 0.003 μmol, ~10 times higher than that for the Fe/N ratio of 1 at 12
212 h, and further increased to ~700 times higher at 132 h.

213 The N₂ production at all Fe/N ratios showed a substantial increase in the first 12 h (Fig. 3(b)), consistent with
214 the drastic decrease in NO₃⁻ concentrations. The highest N₂ production was 82.2 μmol at 108 h for the Fe/N ratio
215 of 6, and this ratio maintained the highest N₂ production throughout the incubation compared to the other Fe/N
216 ratios, apart from at 84 h. At 84 h, 108 h and 132 h, the N₂ production in treatments with Fe/N ratios of 8–10 were
217 lower compared to those in other treatments.

218



219

220 **Fig. 3** N₂O production (a) and N₂ production (b) in the headspace at different Fe/N ratios during the incubation.

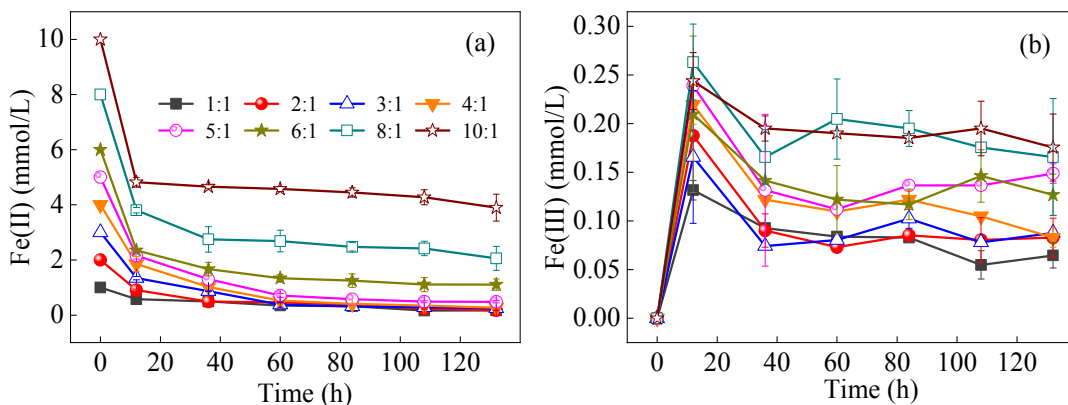
221

222 3.3 Fe(II) oxidation and precipitate characterization

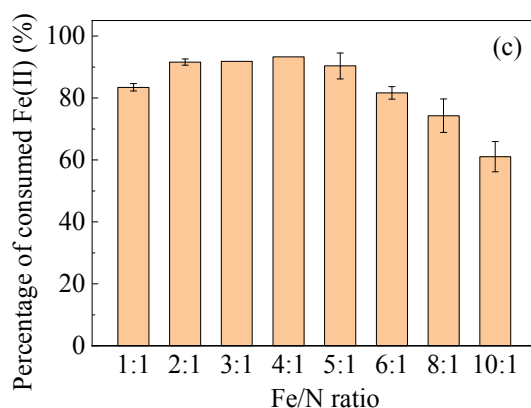
223

224 A rapid oxidation of the aqueous Fe(II) concentration combined with an immediate increase of Fe(III)
 225 concentration was observed at 12 h in the incubation (Fig. 4(a)). In treatments with Fe/N ratios of 1–5, the Fe(II)
 226 oxidation rates followed the pattern of a pseudo-first-order reaction in the first 60 h. The corresponding reaction
 227 rate constants (*k*) were 0.015 h⁻¹ (*R*² = 0.818), 0.023 h⁻¹ (*R*² = 0.723), 0.032 h⁻¹ (*R*² = 0.934), 0.032 h⁻¹ (*R*² =
 228 0.947) and 0.030 h⁻¹ (*R*² = 0.909). A minor decrease in Fe(II) concentrations was observed in all treatments after
 229 60 h. At 132 h, > 82% of the initial Fe(II) had been oxidized at Fe/N ratios of 1–5, and a linear relationship was
 230 observed between N₂ emission (*y*) and Fe(II) concentrations in the medium (*x*) (Fig. A3). The decrease in Fe(II)
 231 concentrations during the incubation ranged from 0.83 mmol/L (at a Fe/N ratio of 1) to 6.10 mmol/L (at a Fe/N
 232 ratio of 10). The Fe(III) concentrations in solution peaked at 12 h, and were lower than 0.26 mmol/L in all the
 233 treatments throughout the experiment (Fig. 4(b)). The % decrease in initial Fe(II) concentrations was higher at
 234 lower Fe/N ratios (Fig. 4(c)), and significant differences in Fe(II) consumption between Fe/N ratios of 1–4 and
 235 Fe/N ratios of 5–10 were observed at 132 h (Table A1).

236



237



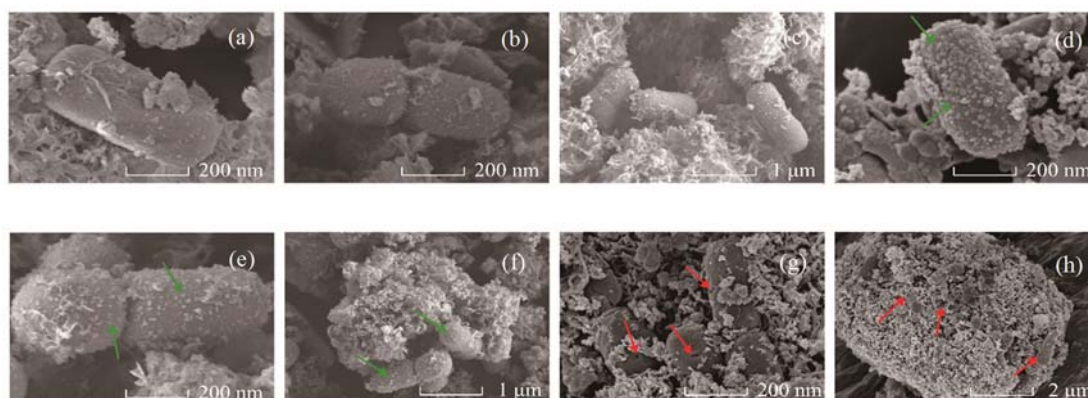
238

239 **Fig. 4** Dissolved Fe(II) concentrations (a), dissolved Fe(III) concentrations (b) during the incubation, and consumption percentages
 240 of Fe(II) at 132 h (c). Values are means ($n = 3$) and error bars in (a), (b) and (c) represent the standard deviation.

241

242 FESEM images showed that the precipitates covering cell surfaces at 60 h were similar among treatments with
 243 Fe/N ratios of 1–3 (Figs. 5(a)–5(c)). Finer precipitates occurred on the cells at Fe/N ratios > 4 (Figs. 5(d)–5(f)).
 244 Small holes were apparent on the surface of cells at a Fe/N ratio of 8 (Figs. 5(g) and 5(h)). Their formation may be
 245 attributed to the accumulation of Fe aggregates on the periplasm and the consequent destruction of the cell
 246 membrane. As a result, the holes would have become visible once the accumulation of Fe aggregates reached a
 247 critical threshold and detached from the cell surface.

248



249

250

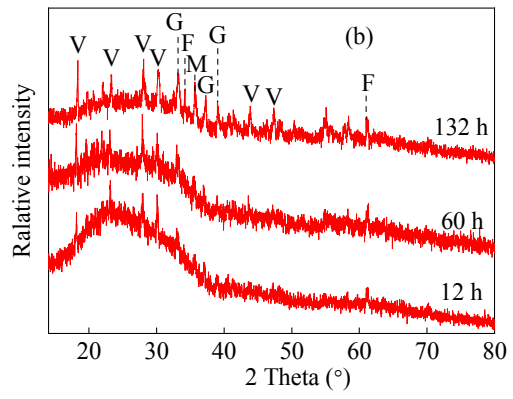
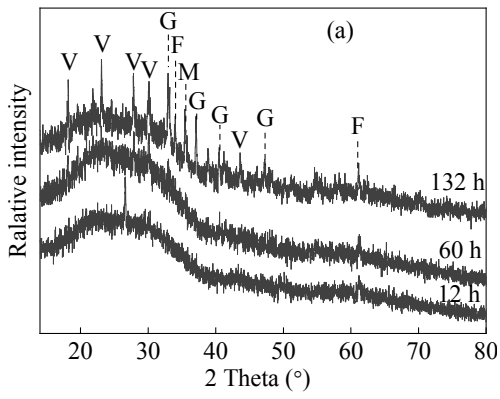
251 **Fig. 5** FESEM images of precipitates from treatments with different Fe/N ratios at 60 h. (a) Fe/N=1:1, (b) Fe/N=2:1, (c) Fe/N=3:1,
 252 (d) Fe/N=4:1, (e) Fe/N=5:1, (f) Fe/N=6:1, (g) Fe/N=8:1 and (h) Fe/N=10:1. Green arrows indicate precipitates, and red arrows
 253 indicate small holes on cell surfaces.

254

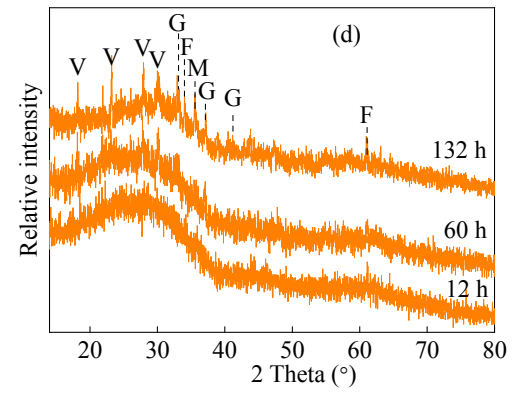
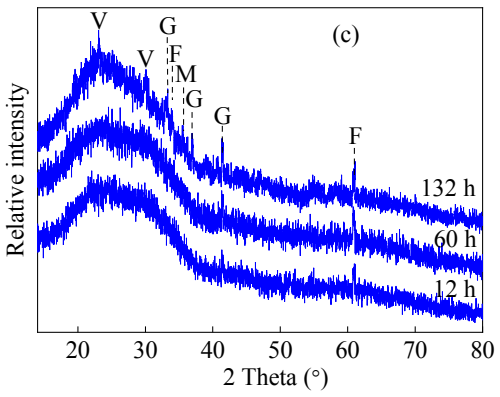
255 For the treatments at Fe/N ratio of 1 and 2, the most obvious peaks in the XRD analysis of the precipitates were
 256 at 132 h, rather than at 12 h and 60 h, while the pattern of peaks was similar in all time steps for treatments of
 257 Fe/N ratios 3–10 (Fig. 6). The XRD patterns showed that the dominant mineral phases in precipitates were
 258 goethite (α -FeOOH) and 2-line ferrihydrite ($\text{Fe}_5\text{HO}_8 \cdot 4\text{H}_2\text{O}$), with two characteristic peaks ($2\theta = 34^\circ, 61^\circ$) (Das et
 259 al., 2011). A marginal fraction was represented by magnetite (Fe_3O_4), which had a characteristic peak at 35.62° .
 260 Some peaks of vivianite ($\text{Fe}_3(\text{PO}_4)_2 \cdot 8\text{H}_2\text{O}$) (Zhao et al., 2013) were identified in all treatments, consistent with the
 261 observation of the white precipitates formation after Fe(II) addition to the medium.

262

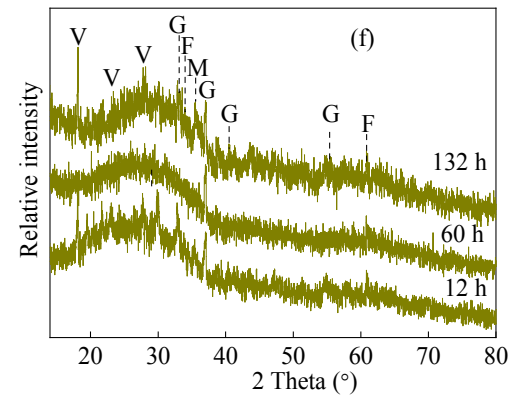
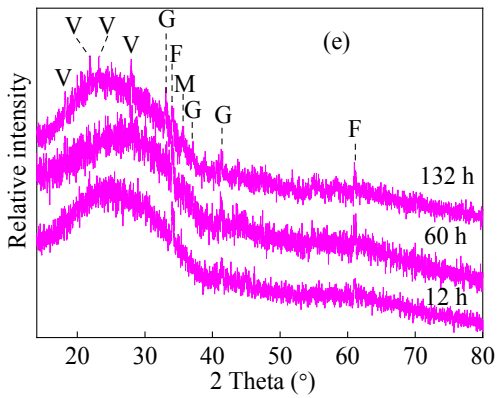
263



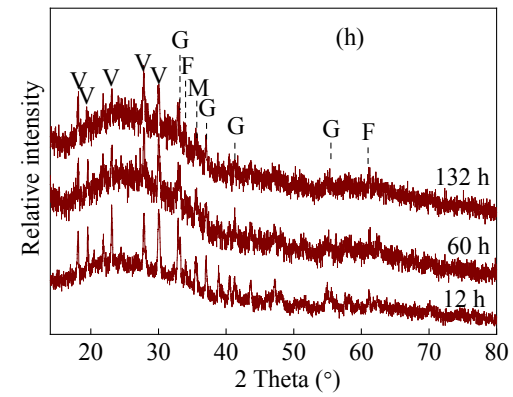
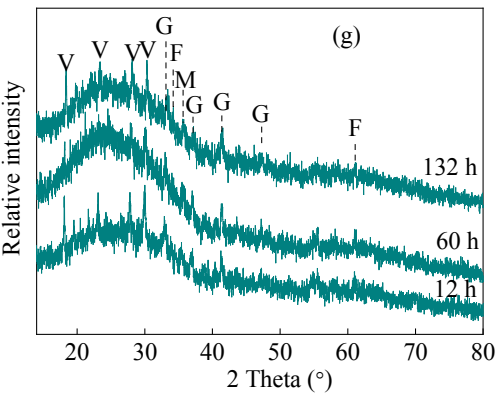
264



265



266



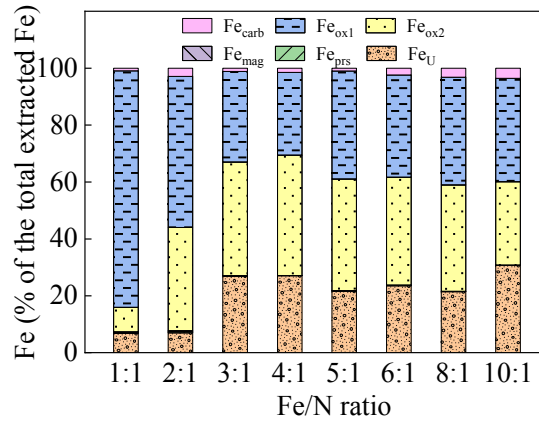
267

268 **Fig. 6** X-ray diffraction patterns of the precipitates from different Fe/N ratio treatments at 12, 60 and 132 h. (a) Fe/N=1:1, (b)
269 Fe/N=2:1, (c) Fe/N=3:1, (d) Fe/N=4:1, (e) Fe/N=5:1, (f) Fe/N=6:1, (g) Fe/N=8:1 and (h) Fe/N=10:1. V represents vivianite, G
270 represents goethite, F represents ferrihydrite and M represents magnetite.

271

272 Total Fe concentrations in the precipitates ranged between 196 and 336 mg/g, and generally increased with the
273 Fe/N ratio (Table A2). The Fe fractions Fe_{ox1} (easily reducible oxides) and Fe_{ox2} (reducible oxides) accounted for
274 the majority of Fe in the precipitates at 132 h (Fig. 7), although the sum percentage of these two fractions
275 generally decreased with increasing Fe/N ratio, from 91.8% at a Fe/N ratio of 1 to 65.5% at a Fe/N ratio of 10.
276 The % of Fe occurring in the unreactive silicate form (Fe_U) generally increased with Fe/N ratio from 6.78% to
277 30.7% at Fe/N ratios of 1 and 10, respectively. Fe_{carb} accounted for the next largest proportion (0.9%–3.5%) in the
278 precipitates at 132 h. The Fe_{mag} content was highest at a Fe/N ratio of 2 (0.39 mg/g) compared to other Fe/N ratios
279 (0.07–0.22 mg/g), in accord with an obvious peak of magnetite at a Fe/N ratio of 2 in the XRD results (Fig. 6(b)),
280 but accounted for a negligible fraction of Fe in the precipitates (< 0.16%). Similarly, poorly reactive sheet silicate
281 (Fe_{prs}) accounted for only 0.03%–0.58% of the total Fe in precipitates after 132 h incubation.

282



283

284 **Fig. 7** Fe speciation of the precipitates from different Fe/N ratio treatments after 132 h incubation. For explanation of the different
285 Fe fractions in the legend see text in Section 2.3.

286

287

288 4 Discussion

289

290 4.1 The fate of N

291

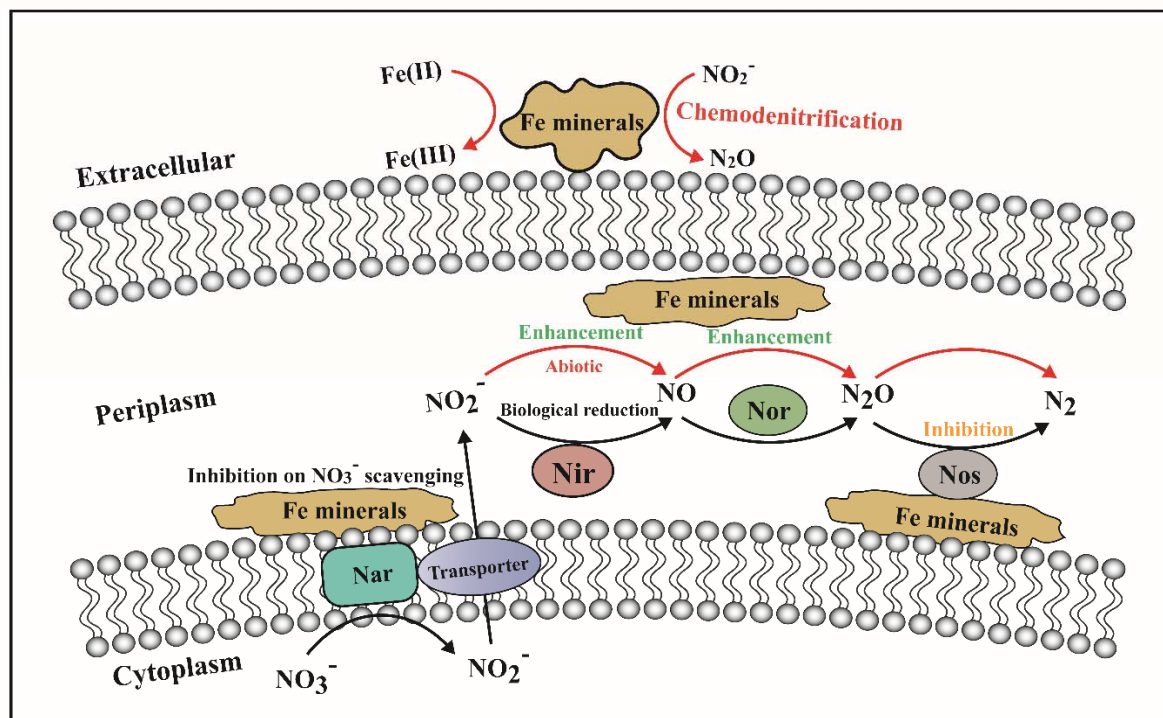
292 NRFO is expected to be an important pathway for N removal in Fe-rich habitats, yielding energy for carbon
293 assimilation into biomass and microbial growth (Weber et al., 2006). The pathways of reduction of NO_3^- and its
294 intermediate products in the current study may include: autotrophic biological reduction with Fe(II) as the electron
295 donor, heterotrophic biological reduction with organic substrates as the electron donor, and abiotic reduction (i.e.,
296 chemodenitrification). In the current mixotrophic incubation, acetate and Fe(II) were both electron donors

297 competing for NO_3^- as the acceptor. Acetate was consumed prior to Fe(II) in NRFO cultures of *Azospira siillum*
298 strain PS under acceptor-limited conditions (Carlson et al., 2013). Although a rapid decrease in the dissolved
299 Fe(II) concentrations occurred at 12 h for all treatments in the current study, it may be due to the production of
300 vivianite (as evidenced by the XRD analysis results, Fig. 6) instead of consumption as an electron donor in NO_3^-
301 reduction.

302 At 132 h, higher Fe(II) consumption accompanied by lower DOC consumption (Fig. A4; Table A1) occurred as
303 Fe/N ratio increased, which could be attributed to the prevention of carbon assimilation by periplasmic Fe
304 encrustation and relative inhibition of heterotrophic biological reduction (Miot et al., 2015) with increasing Fe/N
305 ratio. These tendencies could also be attributed to an increasing role of chemodenitrification or autotrophic
306 biological reduction at higher Fe/N ratios. The lower pH solution values at higher Fe/N ratios (Fig. A2) supported
307 this interpretation as the process of N heterotrophic biological reduction produces alkalinity, in contrast to the
308 production of acidity by chemodenitrification and autotrophic biological reduction (Straub et al., 1996). However,
309 it was not possible in the current study to identify which of the autotrophic biological reduction or
310 chemodenitrification pathways dominated Fe(II) consumption. From a stoichiometric point of view, the oxidation
311 of Fe(II) couldn't provide sufficient electrons for nitrate reduction to N_2 when the Fe/N ratio was less than 5.
312 Organic carbon was consumed to supplement electrons and the consumed organic carbon decreased with the
313 increasing Fe/N ratio (Table A1).

314 Decreasing NO_3^- reduction was observed as Fe/N ratio increased, suggesting that a high Fe/N ratio inhibited the
315 utilization of NO_3^- by *Paracoccus denitrificans*. This finding is aligned with those from other studies so that
316 possible mechanisms for the role of Fe minerals in the NRFO process can be proposed (Fig. 8). Similar
317 experiments conducted in a mixotrophic medium reported that cells were heavily encrusted by Fe minerals at an
318 initial Fe(II) concentration of 8 mmol/L, lost their motility and were unable to utilize acetate and NO_3^- as
319 substrates for heterotrophic growth (Chakraborty et al., 2011). Furthermore, the coverage of Fe aggregates on the
320 cell surface affected cell growth, and even caused the death of cells (Miot et al., 2015). The cell growth is closely
321 related to enzyme activity. Membrane-bound and periplasmic NO_3^- reductase enzymes have been shown to be
322 expressed in *Paracoccus denitrificans*, with the former playing a dominant role in NO_3^- reduction under anaerobic
323 conditions and having an active site in the cytoplasm (Sears et al., 1997). As the insoluble Fe aggregates cannot
324 diffuse into microbial cells, the encrustations of Fe minerals observed in the periplasm could not directly influence
325 the active site of the membrane-bound NO_3^- reductase in the cytoplasm and subsequent denitrification (Sparacino-
326 Watkins et al., 2014). However, the Fe minerals probably inhibited the NO_3^- scavenging ability of cells, and
327 hence probably contributed to the decreased NO_3^- reduction rate (Fig. 8).

328



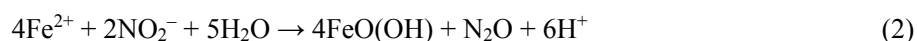
329

330 **Fig. 8** Possible mechanisms for the role of Fe minerals in the NRFO process mediated by bacteria. Chemodenitrification is
 331 indicated by red arrows and biological reduction is indicated by black arrows. Nar, nitrate reductase; Nir, nitrite reductase; Nor, nitric
 332 oxide reductase; Nos, nitrous oxide reductase.

333

334 Differences in NO_2^- accumulation between the different treatments in the current study suggest that the rate of
 335 N reduction after the transformation of NO_3^- to NO_2^- was affected by the Fe/N ratio. Chakraborty et al. (2011)
 336 reported that NO_2^- accumulation occurred only when Fe(II) was present, indicating the inhibiting effect of
 337 concomitant Fe(II) oxidation on NO_2^- reduction during the NRFO process. NO_2^- reductase occurring in the
 338 periplasm (Sears et al., 1997) may become coated by Fe minerals, leading to a decrease in the NO_2^- reduction rate
 339 (Fig. 8) and the accumulation of NO_2^- . If only the negative effect of Fe minerals covering was considered, high
 340 NO_2^- accumulation should have been observed as Fe/N ratio increased. However, NO_2^- accumulation decreased
 341 as Fe/N ratio increased from 2 to 10 (Fig. 2(b)), suggesting some other internal process accelerating NO_2^-
 342 reduction. Indeed, the rapid formation of Fe minerals during the NRFO process may provide a secondary and
 343 presumably faster pathway for NO_2^- reduction (Buchwald et al., 2016), in which Fe minerals can play a positive
 344 role in NO_2^- reduction through chemodenitrification (Eq. (2)), since a strong chemical potential exists between
 345 Fe(II) and NO_2^- (Carlson et al., 2012; Klueglein and Kappler, 2013):

346



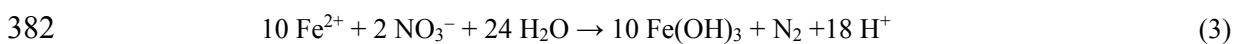
347

348 The Gibbs free energies of Eq. (2) are $-147.6 \text{ kJ/mol e}^-$, indicating that the chemical reactions between Fe(II)
 349 and nitrite are thermodynamically feasible (Liu et al., 2019). Rates of Fe(II) oxidation and NO_2^- reduction for
 350 chemodenitrification were shown to increase simultaneously in the pH range 5.5–7.0 in a study involving pH
 effect and mineral formation on the interaction between NO_2^- and Fe(II) (Chen et al., 2020). In the

351 chemodenitrification process, the reduction of NO_2^- by Fe(II) can be catalyzed by Fe minerals (Fig. 8), such as
352 magnetite and goethite (Buchwald et al., 2016; Grabb et al., 2017). Hence, the Fe minerals produced at high Fe/N
353 ratios can have a dual effect on the NO_2^- reduction process. Fe minerals (e.g., ferrihydrite, goethite and magnetite)
354 on cell surfaces may act to accelerate chemodenitrification, while Fe minerals in the periplasm may inhibit NO_2^-
355 reduction. From biogeochemical modeling of NRFO experiments, Jamieson et al. (2018) showed that
356 chemodenitrification could be responsible for 40% of the overall dissolved Fe(II) oxidized by *Paracoccus*
357 *denitrificans* in media with acetate, with the accompanying biotic NRFO accounting for the remaining oxidation.
358 As more Fe minerals were produced at higher Fe/N ratios than lower ratios, in the current study
359 chemodenitrification probably played a greater role in NO_2^- reduction. In addition, the Fe minerals formed
360 associated with the biologically-mediated component of NRFO (i.e. goethite, and magnetite) differ from those
361 formed by chemodenitrification (only goethite) (Liu et al., 2019).

362 Processes involving N are closely associated with greenhouse gas emissions (He et al., 2017), and thus it is
363 important to know the effect of the Fe/N ratio on the NRFO process with regards to yield of N_2O , one of the
364 products of chemodenitrification (Eq. (2)). Chemodenitrification accounted for 15%–25% of the total N_2O
365 production from marine sediments, indicating the importance of N_2O production from chemodenitrification (Otte
366 et al., 2019). In the current study, the occurrence of the highest N_2O accumulation in the high Fe/N ratio
367 treatments was attributed to enhanced chemodenitrification and NO_2^- reduction due to the high Fe(II)
368 concentrations. Although the observed N_2O production was much lower than the N_2 production, it has important
369 implications for the greenhouse effect as the global warming potential of N_2O is 300 times that of CO_2 on a 100-
370 year scale (Thakur and Medhi, 2019). Hence, NRFO processes may be notable sources of N_2O in Fe-rich habitats.
371 Although enzymatic denitrification can reduce N_2O to N_2 under anoxic conditions (Zhu-Barker et al., 2015), the
372 higher N_2O accumulations in the high Fe/N ratio treatments in the current study indicate that enzymatic
373 denitrification in the transformation of N_2O to N_2 was inhibited (Fig. 8). This could be attributed to a decrease of
374 the metabolic capabilities of these bacteria at high Fe/N ratios, caused by the precipitation and encrustation of Fe
375 (Chakraborty et al., 2011; Liu et al., 2019).

376 At 132 h, the dominant N denitrification product was N_2 , which accounted for $\geq 56\%$ of the reduced NO_3^- in all
377 Fe/N ratio treatments (Fig. 9). Hence, in oxygen minimum zones an appreciable amount of N_2 emission is a
378 promising way to permanently remove reactive N from Fe-rich habitats. The highest N_2 production (Fig. 3(b)) and
379 percentage N_2 of reduced NO_3^- (81.2% at 132 h) occurred at a Fe/N ratio of 6, where the actual ratio between
380 Fe(II) oxidation and the net NO_3^- reduction was 5.37, close to the theoretical value that can be obtained from Eq.
381 (3) (Straub et al., 1996) for NRFO organisms:



383 Considering that the formation of N_2O has a negative effect on the atmosphere, while complete denitrification
384 with the formation of N_2 has almost no effect (Włodarczyk et al., 2019), a Fe/N molar ratio of 6 is the optimum
385 for formation of N_2 , to ensure the most complete denitrification process.

386 The observed N_2 production in the treatments with Fe/N ratios of 8–10 were lower than that in other treatments
387 (Fig. 9), and was attributed to that further enzymatic reduction of N_2O to N_2 was likely severely hampered at high
388 Fe/N ratios due to coating of cells with Fe minerals (Fig. 8).

389

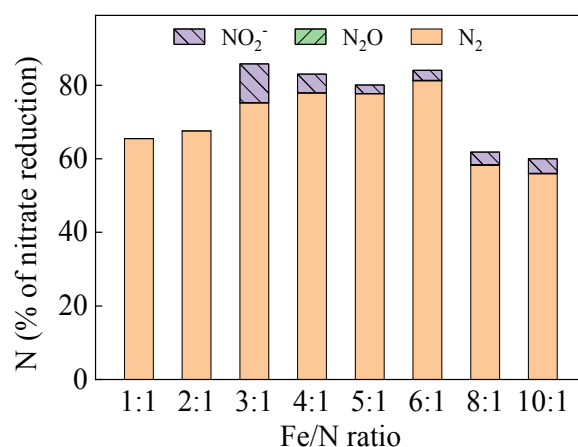


Fig. 9 Percentage contribution of the N products of denitrification (NO₂⁻, N₂O and N₂) to NO₃⁻ reduction from different Fe/N ratio treatments after 132 h incubation.

4.2 Fe transformation

NRFO bacteria have been demonstrated to oxidize both soluble and insoluble Fe(II) (Carlson et al., 2012). Vivianite with a K_{sp} of 10^{-36} is a very stable Fe(II) mineral (Miot et al., 2009a), although it has been shown to be oxidized (~0.5 mmol Fe(II) over 24 h) by *Acidovorax ebreus*, but only in the presence of an organic cosubstrate (Carlson et al., 2013). The vivianite detected in precipitates in the current study might not be utilized, especially at high Fe/N ratios, as the Fe minerals produced during NRFO has a very low solubility at circumneutral pH (Jamieson et al., 2018). Furthermore, the solubility of Fe(III) increases with decreasing pH values (Weber et al., 2006), probably accounting for the occurrence of the highest concentrations of Fe(III) in solution in the current study in the treatments with the higher Fe/N ratios and also the lower pH (Fig. 4(b), Fig. A2). Apart from pH, the concentration of Fe(III) in solution was also affected by the type of Fe(III) minerals; the soluble Fe concentration of ferrihydrite and goethite at pH 7 is $10^{-3.1}$ $\mu\text{mol/L}$ and $10^{-10.9}$ – $10^{-5.9}$ $\mu\text{mol/L}$, respectively (Schwertmann, 1991). Meanwhile, the oxidation of Fe(II) species during the NRFO process can result in the precipitation of a variety of Fe(III) minerals (Liu et al., 2019). With strong complexing ligands (e.g., CO₃²⁻) in the system, precipitated Fe tends to form goethite (Bryce et al., 2018). In the current anoxic systems, the formation of goethite was observed at 60 h and 132 h in the treatments with high Fe/N ratios.

The combination of XRD analysis and sequential extraction for Fe fractions is helpful to better understand the type and amount of different Fe minerals produced during the incubation. The pH of the medium solution decreased from an initial value of 7 to 6.14–6.78 across all treatments over 132 h, with the greatest decrease occurring in the high Fe/N ratio treatments (Fig. A2), in accordance with the probable reactions based on stoichiometry (Ottley et al., 1997). In a slightly acidic anoxic environment, the ionization of HCO₃⁻ (initial concentration = 22 mmol/L) can produce very small amounts of CO₃²⁻, which in turn combine with Fe(II) to form FeCO₃. Interestingly, the formation of Fe_{carb} including siderite and ankerite (Poulton and Canfield, 2005) seems to occur only in anoxic habits that are rich in Fe, non-sulfidic, and have a high CO₃²⁻ content (Aller et al., 2004). Easily reducible oxides (Fe_{ox1}) include ferrihydrite and lepidocrocite, while reducible oxides (Fe_{ox2}) include goethite, hematite, and akaganéite (Poulton and Canfield, 2005). Taken together, the results of the XRD analysis and sequential extraction indicated that Fe_{ox1} and Fe_{ox2} in the precipitates included ferrihydrite and goethite,

421 respectively. The Fe_{ox1} fraction accounted for 83.1% and 53.1% of the total Fe in precipitates in the Fe/N ratio
422 treatments of 1 and 2, respectively, showing that easily reducible oxides was the main Fe mineral produced during
423 the NRFO process at Fe/N ratios of 1–2. At Fe/N ratios of 3–10, percentages of the total Fe in precipitates were
424 similar for Fe_{ox1} (29.1%–37.9%) and Fe_{ox2} (29.3%–42.3%), suggesting the dominant Fe minerals were easily
425 reducible oxides and reducible oxides. A marginal amount of Fe_{mag} (0.02%–0.16%) was observed by sequential
426 extraction of Fe precipitates across all treatments, and magnetite was also identified by XRD. The presence of
427 vivianite was detected in the precipitates by XRD analysis, but the sequential extraction procedure used in the
428 current study was not suitable to specifically identify vivianite. Different Fe minerals have different capacities for
429 combining with contaminants such as metal/metalloids and phosphorus, and thus play different roles in aquatic
430 geochemistry. Hence, the interaction between the Fe/N ratio and NRFO processes may influence not only NO₃⁻
431 reduction but also the quantity and composition of Fe oxidation products with different environmental behavior.
432 The results may shed light on the denitrification characteristics and Fe transformation process mediated by Fe/N
433 molar ratios in Fe-rich anoxic zones in both natural aquatic environments and wastewater treatment systems.

434

435

436 5 Conclusions

437

438 NO₃⁻ reduction coupled with Fe(II) oxidation was mediated by *Paracoccus denitrificans* in incubation
439 experiments of 132 h duration, with different initial Fe/N molar ratios. NO₃⁻ reduction decreased as the Fe/N ratio
440 increased from 1 to 10. Considerable NO₂⁻ accumulation, equivalent to > 30% of the reduced NO₃⁻, was observed
441 at Fe/N ratios of 2–5 within 60 h. N₂O emissions increased notably with increasing Fe/N ratios. Maximum
442 production of N₂ occurred at an initial Fe/N molar ratio of 6, higher than at other Fe/N ratios investigated, and
443 accounted for 81.2% of the reduction of NO₃⁻. Ferrihydrite, goethite, vivianite and magnetite were identified by
444 XRD in Fe precipitates sampled after 132 h. The dominant Fe minerals were easily reducible oxides at Fe/N ratios
445 of 1–2, and easily reducible oxides and reducible oxides at Fe/N ratios of 3–10.

446

447

448 Acknowledgements This work was supported by the National Key R & D Program of China (No.
449 2017YFC0505305) and the Fundamental Research Funds for the Central Universities (No. 2662018JC053).

450

451

452 **Electronic Supplementary material** Supplementary material is available in the online version of this article at
453 <https://doi.org/10.1007/s11783-020-1366-2> and is accessible for authorized users.

454

455

456 References

457

458 Aller R C, Heilbrun C, Panzeca C, Zhu Z, Baltzer F (2004). Coupling between sedimentary dynamics, early diagenetic processes, and
459 biogeochemical cycling in the Amazon-Guianas mobile mud belt: Coastal French Guiana. *Marine Geology*, 208(2–4): 331–360
460 doi:10.1016/j.margeo.2004.04.027

461 APHA (2012). Standard Methods for the Examination of Water and Wastewater, 22nd ed. Washington, DC: American Public Health
462 Association

463 Bryce C, Blackwell N, Schmidt C, Otte J, Huang Y M, Kleindienst S, Tomaszewski E, Schad M, Warter V, Peng C, Byrne J M, Kappler A
464 (2018). Microbial anaerobic Fe(II) oxidation: Ecology, mechanisms and environmental implications. *Environmental Microbiology*, 20(10):
465 3462–3483 doi:10.1111/1462-2920.14328

466 Buchwald C, Grabb K, Hansel C M, Wankel S D (2016). Constraining the role of iron in environmental nitrogen transformations: Dual stable
467 isotope systematics of abiotic NO₂⁻ reduction by Fe(II) and its production of N₂O. *Geochimica et Cosmochimica Acta*, 186: 1–12
468 doi:10.1016/j.gca.2016.04.041

469 Carlson H K, Clark I C, Melnyk R A, Coates J D (2012). Toward a mechanistic understanding of anaerobic nitrate-dependent iron oxidation:
470 Balancing electron uptake and detoxification. *Frontiers in Microbiology*, 3: 57 doi:10.3389/fmicb.2012.00057

471 Carlson H K, Clark I C, Blazewicz S J, Iavarone A T, Coates J D (2013). Fe(II) oxidation is an innate capability of nitrate-reducing bacteria
472 that involves abiotic and biotic reactions. *Journal of Bacteriology*, 195(14): 3260–3268 doi:10.1128/JB.00058-13

473 Chakraborty A, Roden E E, Schieber J, Picardal F (2011). Enhanced growth of *Acidovorax* sp. strain 2AN during nitrate-dependent Fe(II)
474 oxidation in batch and continuous-flow systems. *Applied and Environmental Microbiology*, 77(24): 8548–8556 doi:10.1128/AEM.06214-11

475 Chen D D, Liu T X, Li X M, Li F B, Luo X B, Wu Y D, Wang Y (2018). Biological and chemical processes of microbially mediated nitrate-
476 reducing Fe(II) oxidation by *Pseudogulbenkiania* sp. strain 2002. *Chemical Geology*, 476: 59–69 doi:10.1016/j.chemgeo.2017.11.004

477 Chen D D, Yuan X, Zhao W Q, Luo X B, Li F B, Liu T X (2020). Chemodenitrification by Fe(II) and nitrite: pH effect, mineralization and
478 kinetic modeling. *Chemical Geology*, 541: 119586 doi:10.1016/j.chemgeo.2020.119586

479 Das S, Hendry M J, Essilfie-Dughan J (2011). Transformation of two-line ferrihydrite to goethite and hematite as a function of pH and
480 temperature. *Environmental Science & Technology*, 45(1): 268–275 doi:10.1021/es101903y

481 Ehrenreich A, Widdel F (1994). Anaerobic oxidation of ferrous iron by purple bacteria, a new type of phototrophic metabolism. *Applied and*
482 *Environmental Microbiology*, 60(12): 4517–4526 doi:10.1128/AEM.60.12.4517-4526.1994

483 Grabb K C, Buchwald C, Hansel C M, Wankel S D (2017). A dual nitrite isotopic investigation of chemodenitrification by mineral-
484 associated Fe(II) and its production of nitrous oxide. *Geochimica et Cosmochimica Acta*, 196: 388–402 doi:10.1016/j.gca.2016.10.026

485 Han Z F, Miao Y, Dong J, Shen Z Q, Zhou Y X, Liu S, Yang C P (2019). Enhanced nitrogen removal and microbial analysis in partially
486 saturated constructed wetland for treating anaerobically digested swine wastewater. *Frontiers of Environmental Science & Engineering*,
487 13(4): 52 doi:10.1007/s11783-019-1133-4

488 He Q, Zhu Y Y, Li G, Fan L L, Ai H N, Huangfu X L, Li H (2017). Impact of dissolved oxygen on the production of nitrous oxide in
489 biological aerated filters. *Frontiers of Environmental Science & Engineering*, 11(6): 16 doi:10.1007/s11783-017-0964-0

490 Jamieson J, Prommer H, Kaksonen A H, Sun J, Siade A J, Yusov A, Bostick B (2018). Identifying and quantifying the intermediate
491 processes during nitrate-dependent iron(II) oxidation. *Environmental Science & Technology*, 52(10): 5771–5781
492 doi:10.1021/acs.est.8b01122

493 Klueglein N, Kappler A (2013). Abiotic oxidation of Fe(II) by reactive nitrogen species in cultures of the nitrate-reducing Fe(II) oxidizer
494 *Acidovorax* sp. BoFeN1 - questioning the existence of enzymatic Fe(II) oxidation. *Geobiology*, 11(2): 180–190 doi:10.1111/gbi.12019

495 Larese-Casanova P, Haderlein S B, Kappler A (2010). Biomineralization of lepidocrocite and goethite by nitrate-reducing Fe(II)-oxidizing
496 bacteria: Effect of pH, bicarbonate, phosphate, and humic acids. *Geochimica et Cosmochimica Acta*, 74(13): 3721–3734
497 [doi:10.1016/j.gca.2010.03.037](https://doi.org/10.1016/j.gca.2010.03.037)

498 Liu T X, Chen D D, Luo X B, Li X M, Li F B (2019). Microbially mediated nitrate-reducing Fe(II) oxidation: Quantification of
499 chemodenitrification and biological reactions. *Geochimica et Cosmochimica Acta*, 256: 97–115 [doi:10.1016/j.gca.2018.06.040](https://doi.org/10.1016/j.gca.2018.06.040)

500 Ma H, Zhao B Y, Li L, Xie F, Zhou H J, Zheng Q, Wang X H, He J, Lu C W (2019). Fractionation trends of phosphorus associating with
501 iron fractions: An explanation by the simultaneous extraction procedure. *Soil & Tillage Research*, 190: 41–49 [doi:10.1016/j.still.2019.02.012](https://doi.org/10.1016/j.still.2019.02.012)

502 Melton E D, Swanner E D, Behrens S, Schmidt C, Kappler A (2014). The interplay of microbially mediated and abiotic reactions in the
503 biogeochemical Fe cycle. *Nature Reviews. Microbiology*, 12(12): 797–808 [doi:10.1038/nrmicro3347](https://doi.org/10.1038/nrmicro3347)

504 Miot J, Benzerara K, Morin G, Bernard S, Beyssac O, Larquet E, Kappler A, Guyot F (2009a). Transformation of vivianite by anaerobic
505 nitrate-reducing iron-oxidizing bacteria. *Geobiology*, 7(3): 373–384 [doi:10.1111/j.1472-4669.2009.00203.x](https://doi.org/10.1111/j.1472-4669.2009.00203.x)

506 Miot J, Benzerara K, Morin G, Kappler A, Bernard S, Obst M, Féraud C, Skouri-Panet F, Guigner J M, Posth N, Galvez M, Brown G E Jr,
507 Guyot F (2009b). Iron biomineralization by anaerobic neutrophilic iron-oxidizing bacteria. *Geochimica et Cosmochimica Acta*, 73(3): 696–
508 711 [doi:10.1016/j.gca.2008.10.033](https://doi.org/10.1016/j.gca.2008.10.033)

509 Miot J, Remusat L, Duprat E, Gonzalez A, Pont S, Poinso M (2015). Fe biomineralization mirrors individual metabolic activity in a nitrate-
510 dependent Fe(II)-oxidizer. *Frontiers in Microbiology*, 6: 879 [doi:10.3389/fmicb.2015.00879](https://doi.org/10.3389/fmicb.2015.00879)

511 Muehe E M, Gerhardt S, Schink B, Kappler A (2009). Ecophysiology and the energetic benefit of mixotrophic Fe(II) oxidation by various
512 strains of nitrate-reducing bacteria. *FEMS Microbiology Ecology*, 70(3): 335–343 [doi:10.1111/j.1574-6941.2009.00755.x](https://doi.org/10.1111/j.1574-6941.2009.00755.x)

513 Otte J M, Blackwell N, Ruser R, Kappler A, Kleindienst S, Schmidt C (2019). N₂O formation by nitrite-induced (chemo)denitrification in
514 coastal marine sediment. *Scientific Reports*, 9: 10691 [doi:10.1038/s41598-019-47172-x](https://doi.org/10.1038/s41598-019-47172-x)

515 Ottley C J, Davison W, Edmunds W M (1997). Chemical catalysis of nitrate reduction by iron(II). *Geochimica et Cosmochimica Acta*, 61(9):
516 1819–1828 [doi:10.1016/S0016-7037\(97\)00058-6](https://doi.org/10.1016/S0016-7037(97)00058-6)

517 Picardal F (2012). Abiotic and microbial interactions during anaerobic transformations of Fe(II) and NO₃⁻. *Frontiers in Microbiology*, 3: 112
518 [doi:10.3389/fmicb.2012.00112](https://doi.org/10.3389/fmicb.2012.00112)

519 Posth N R, Canfield D E, Kappler A (2014). Biogenic Fe(III) minerals: From formation to diagenesis and preservation in the rock record.
520 *Earth-Science Reviews*, 135: 103–121 [doi:10.1016/j.earscirev.2014.03.012](https://doi.org/10.1016/j.earscirev.2014.03.012)

521 Poulton S W, Canfield D E (2005). Development of a sequential extraction procedure for iron: Implications for iron partitioning in
522 continentally derived particulates. *Chemical Geology*, 214(3–4): 209–221 [doi:10.1016/j.chemgeo.2004.09.003](https://doi.org/10.1016/j.chemgeo.2004.09.003)

523 Pownceby M I, Hapugoda S, Manuel J, Webster N A S, MacRae C M (2019). Characterisation of phosphorus and other impurities in
524 goethite-rich iron ores: Possible P incorporation mechanisms. *Minerals Engineering*, 143: 106022 [doi:10.1016/j.mineng.2019.106022](https://doi.org/10.1016/j.mineng.2019.106022)

525 Schwertmann U (1991). Solubility and dissolution of iron oxides. *Plant and Soil*, 130(1–2): 1–25 [doi:10.1007/BF00011851](https://doi.org/10.1007/BF00011851)

526 Sears H J, Spiro S, Richardson D J (1997). Effect of carbon substrate and aeration on nitrate reduction and expression of the periplasmic and
527 membrane-bound nitrate reductases in carbon-limited continuous cultures of *Paracoccus denitrificans* Pd1222. *Microbiology-UK*, 143(12):
528 3767–3774 [doi:10.1099/00221287-143-12-3767](https://doi.org/10.1099/00221287-143-12-3767)

529 Sparacino-Watkins C, Stolz J F, Basu P (2014). Nitrate and periplasmic nitrate reductases. *Chemical Society Reviews*, 43(2): 676–706
530 [doi:10.1039/C3CS60249D](https://doi.org/10.1039/C3CS60249D)

531 Stookey L L (1970). Ferrozine: A new spectrophotometric reagent for iron. *Analytical Chemistry*, 42(7): 779–781 [doi:10.1021/ac60289a016](https://doi.org/10.1021/ac60289a016)

532 Straub K L, Benz M, Schink B, Widdel F (1996). Anaerobic, nitrate-dependent microbial oxidation of ferrous iron. *Applied and*
533 *Environmental Microbiology*, 62(4): 1458–1460 [doi:10.1128/AEM.62.4.1458-1460.1996](https://doi.org/10.1128/AEM.62.4.1458-1460.1996)

534 Thakur I S, Medhi K (2019). Nitrification and denitrification processes for mitigation of nitrous oxide from waste water treatment plants for
535 biovalorization: Challenges and opportunities. *Bioresource Technology*, 282: 502–513 [doi:10.1016/j.biortech.2019.03.069](https://doi.org/10.1016/j.biortech.2019.03.069)

536 Vasilaki V, Volcke E I P, Nandi A K, van Loosdrecht M C M, Katsou E (2018). Relating N₂O emissions during biological nitrogen removal
537 with operating conditions using multivariate statistical techniques. *Water Research*, 140: 387–402 [doi:10.1016/j.watres.2018.04.052](https://doi.org/10.1016/j.watres.2018.04.052)

538 Wang M L, Hu R G, Zhao J S, Kuzyakov Y, Liu S R (2016). Iron oxidation affects nitrous oxide emissions via donating electrons to
539 denitrification in paddy soils. *Geoderma*, 271: 173–180 [doi:10.1016/j.geoderma.2016.02.022](https://doi.org/10.1016/j.geoderma.2016.02.022)

540 Watsuntorn W, Ruangchainikom C, Rene E R, Lens P N L, Chulalaksananukul W (2019). Comparison of sulphide and nitrate removal from
541 synthetic wastewater by pure and mixed cultures of nitrate-reducing, sulphide-oxidizing bacteria. *Bioresource Technology*, 272: 40–47
542 [doi:10.1016/j.biortech.2018.09.125](https://doi.org/10.1016/j.biortech.2018.09.125)

543 Weber K A, Achenbach L A, Coates J D (2006). Microorganisms pumping iron: Anaerobic microbial iron oxidation and reduction. *Nature*
544 *Reviews. Microbiology*, 4(10): 752–764 [doi:10.1038/nrmicro1490](https://doi.org/10.1038/nrmicro1490)

545 Włodarczyk T, Balakhnina T, Matichenkov V, Brzezińska M, Nosalewicz M, Szarlip P, Fomina I (2019). Effect of silicon on barley growth
546 and N₂O emission under flooding. *Science of the Total Environment*, 685: 1–9 [doi:10.1016/j.scitotenv.2019.05.410](https://doi.org/10.1016/j.scitotenv.2019.05.410)

547 Zhang L H, Zheng J, Guo J B, Guan X H, Zhu S Y, Jia Y P, Zhang J, Zhang X Y, Zhang H F (2019). Effects of Al³⁺ on pollutant removal
548 and extracellular polymeric substances (EPS) under anaerobic, anoxic and oxic conditions. *Frontiers of Environmental Science &*
549 *Engineering*, 13(6): 85 [doi:10.1007/s11783-019-1169-5](https://doi.org/10.1007/s11783-019-1169-5)

550 Zhang M, Zheng P, Li W, Wang R, Ding S, Abbas G (2015). Performance of nitrate-dependent anaerobic ferrous oxidizing (NAFO) process:
551 A novel prospective technology for autotrophic denitrification. *Bioresource Technology*, 179: 543–548 [doi:10.1016/j.biortech.2014.12.036](https://doi.org/10.1016/j.biortech.2014.12.036)

552 Zhang M, Zheng P, Wang R, Li W, Lu H F, Zhang J Q (2014). Nitrate-dependent anaerobic ferrous oxidation (NAFO) by denitrifying
553 bacteria: A perspective autotrophic nitrogen pollution control technology. *Chemosphere*, 117: 604–609
554 [doi:10.1016/j.chemosphere.2014.09.029](https://doi.org/10.1016/j.chemosphere.2014.09.029)

555 Zhao L D, Dong H L, Kukkadapu R, Agrawal A, Liu D, Zhang J, Edelmann R E (2013). Biological oxidation of Fe(II) in reduced nontronite
556 coupled with nitrate reduction by *Pseudogulbenkiania* sp. Strain 2002. *Geochimica et Cosmochimica Acta*, 119: 231–247
557 [doi:10.1016/j.gca.2013.05.033](https://doi.org/10.1016/j.gca.2013.05.033)

558 Zhu-Barker X, Cavazos A R, Ostrom N E, Horwath W R, Glass J B (2015). The importance of abiotic reactions for nitrous oxide production.
559 *Biogeochemistry*, 126(3): 251–267 [doi:10.1007/s10533-015-0166-4](https://doi.org/10.1007/s10533-015-0166-4)

560 Zorgani E A, Cibati A, Trois C (2016). Assessment of a natural iron-based sand for the removal of nitrate from water. *Water, Air, and Soil*
561 *Pollution*, 227(7): 249 [doi:10.1007/s11270-016-2942-8](https://doi.org/10.1007/s11270-016-2942-8)

562

563